

This is the accepted manuscript made available via CHORUS. The article has been published as:

Effects of stochastic time-delayed feedback on a dynamical system modeling a chemical oscillator

Héctor O. González Ochoa, Gualberto Solís Perales, Irving R. Epstein, and Ricardo Femat

Phys. Rev. E **97**, 052214 — Published 23 May 2018

DOI: [10.1103/PhysRevE.97.052214](https://doi.org/10.1103/PhysRevE.97.052214)

Effects of stochastic time-delayed feedback on a dynamical system modelling a chemical oscillator

Héctor O. González Ochoa* and Gualberto Solís Perales

Departamento de Electrónica, Universidad de Guadalajara.

Av. Revolución 1500, 44430, Guadalajara Jal, México

Irving R. Epstein

Department of Chemistry, Brandeis University, Waltham, MA 02454-9110, USA

Ricardo Femat

Instituto Potosino de Investigación Científica y Tecnológica A.C., San Luis Potosí, México

(Dated: March 26, 2018)

Abstract

We examine how stochastic time-delayed negative feedback affects the dynamical behavior of a model oscillatory reaction. We apply constant and stochastic time-delayed negative feedbacks to a point Field-Körös-Noyes (FKN) photosensitive oscillator and compare their effects. Negative feedback is applied in the form of simulated inhibitory electromagnetic radiation with an intensity proportional to the concentration of oxidized light-sensitive catalyst in the oscillator. We first characterize the system under non-delayed inhibitory feedback; then we explore and compare the effects of constant (deterministic) *vs.* stochastic time-delayed feedback. We find that the oscillatory amplitude, frequency and waveform are essentially preserved when low-dispersion stochastic delayed feedback is used, whereas small but measurable changes appear when a large dispersion is applied.

* hector.tnh@gmail.com

I. INTRODUCTION

Oscillatory chemical reactions show complex nonlinear phenomena with a rich diversity of patterns, many resembling those found in biological processes. For instance, striking similarities can be noted in wave patterns displayed by the Belousov-Zhabotinsky (BZ) reaction [1–5], starving amoeba *Dictyostelium discoideum* [6] and calcium waves in *Xenopus laevis* oocytes [7, 8]. Turing was the first to propose reaction-diffusion as a possible underlying mechanism in the process of morphogenesis [9]. The structures predicted by Turing have been experimentally observed in both continuous [10] and cell-compartmentalized chemical systems [11]. Chemical oscillators are reaction-diffusion systems, which have been proposed and used as model systems for elucidating complex biomimetic dynamics [11–14]. The BZ reaction is the prototypical chemical oscillator in such investigations. The reaction, which occurs in acidic aqueous solution, consists of the oscillatory oxidation by bromate of an organic substrate, usually malonic acid, catalyzed by metal ions or metallo-complexes. A photosensitive version of the BZ reaction, which uses the light-sensitive complex $\text{Ru}(\text{bpy})_3$ as the metal catalyst, can be modulated by the application of an inhibiting electromagnetic field [15, 16]. Richard J. Field, Endre Körös and Richard M. Noyes performed, on the grounds of chemical kinetics, a detailed analysis of the BZ reaction and developed a mechanism, the FKN, (after Field-Körös-Noyes) to account for its oscillatory behavior [17]. The FKN mechanism identifies 11 principle reactions and 12 chemical species and successfully reproduces the behavior of the BZ reaction [18]. Later, the model was extended to include photoinhibition [16, 19, 20].

The application of feedback to a nonlinear dynamical system can induce complex behavior. Feedback can also be used as a control mechanism to drive the system toward a desired dynamics. Different feedback strategies have been explored. Time-delayed feedback has demonstrated its efficacy in controlling chaotic systems [21, 22] since this approach was introduced by Ott and coworkers [23] and later by Pyragas [24]. Additionally, delayed feedback has been used to suppress relaxation oscillations [25], synchronize ensembles of coupled oscillators [26], and investigate emergent dynamics in mechanical [27] and optoelectronic [28] systems. This technique has also been investigated in chemical and biological

systems in both, pointlike and spatially extended diffusive systems. Time-delayed feedback was applied to control unstable orbits in the oscillatory BZ reaction [29]. A rich diversity of spatiotemporal patterns has been investigated by the use of differential-difference equations in a one-species reaction-diffusion system with delay [30]. Control of spatiotemporal chaotic patterns has been attained in the reaction-diffusion Gray-Scott two-species model by means of time-delayed feedback [31]. This strategy can be harnessed to induce pattern transitions [32], spiral waves and their modulation [33], and complex dynamics of localized structures [34] and Turing patterns [35] in reaction diffusion systems. The emergence of spatial patterns triggered by a time delay via a Hopf bifurcation is observed in a plankton prey-predator model [36]. The combination of noise, inherent to any physical system, with time delay in the feedback applied to oscillatory systems can induce undesirable oscillations [25, 37], phenomenon observed in different systems [38–40]. The introduction of a second feedback loop with delay has been applied to stabilize the system or suppress the undesirable dynamics [41–43].

The application of global feedback has been investigated with oscillatory systems [44], coupled oscillator networks [45, 46], and spatially distributed reaction-diffusion systems [47, 48]. The combination of time-delayed with global feedback has been explored in chemical systems [49] and oscillator arrays [50]. Double delayed feedback [51], event-triggered feedback [52] and variable delay feedback [53] have been also explored. The above investigations have employed negative feedback, positive feedback or both.

Time delays can arise from finite time propagation and processing of signals. A reasonable assumption in systems with time-delayed feedback is that in real processes time delay will not be deterministic, but in general will undergo stochastic fluctuations as a consequence of uncontrolled variables or perturbations. This is particularly important in synchronization processes when the intended synchronizing elements do not share a unique time delay in their feedback. Nevertheless, in the active and diverse field of research on feedback, to our knowledge there have been no previous investigations of the role of feedback with stochastic time delay and its effects on system dynamics. We investigate here the behavior of a model chemical oscillator subjected to a time-delayed negative feedback where the delay time is stochastic with a known probability distribution and compare our results with the effects

of a deterministic time delay. We perform numerical experiments on the photosensitive FKN mechanism augmented with inhibitory electromagnetic radiation to study the effects of applying a negative feed-back (NFB). The light intensity is set proportional to the instantaneous concentration of photosensitive catalyst in the reaction, and we choose the normal and Gumbel distributions for the stochastic time delay.

II. SIMULATION

We investigate the effect of time-delayed feedback on the dynamics of the FKN mechanism with photoinhibition. NFB is applied as an inhibitory electromagnetic radiation field on a point FKN oscillator. An experimental realization approximating a point FKN oscillator is a small drop [54, 55] or a continuously stirred tank reactor containing the BZ reaction [56]. The complete model used in the simulations is presented in equations (1–10), which include time-delayed feedback by photoinhibition.

$$\dot{x}_1 = -k_1x_1x_2 + k_2x_2 - 2k_3x_1^2 - k_4x_1 + k_rx_6^2 + k_{red}x_6x_7, \quad (1)$$

$$\dot{x}_2 = -k_1x_1x_2 - k_2x_2 - k_5x_2x_4 + k_6x_5 + k_7x_5 + k_9x_3 + \phi, \quad (2)$$

$$\dot{x}_3 = k_{red}x_6x_7 - k_9x_3 - k_{10}x_3 + \phi, \quad (3)$$

$$\dot{x}_4 = 2k_1x_1x_2 + k_2x_2 + k_3x_1^2 - k_5x_2x_4 + k_6x_5 - k_8x_4, \quad (4)$$

$$\dot{x}_5 = k_5x_2x_4 - k_6x_5 - k_7x_5, \quad (5)$$

$$\dot{x}_6 = 2k_4x_1 - 2k_rx_6^2 - k_{red}x_6x_7, \quad (6)$$

$$\dot{x}_7 = -k_{red}x_6x_7 + k_9x_3 + k_{10}x_3 - \phi, \quad (7)$$

$$\phi(x, t) = k(I)x_7b/(b_C + b), \quad (8)$$

$$k(I) = q_1I, \quad (9)$$

$$I = q_2x_3(t - \tau). \quad (10)$$

The ordinary differential equations (1–7), excluding the function ϕ , are generated from the original FKN mechanism under mass action kinetics and constitute an adequate model

of the BZ reaction. Here $x_1 = [\text{HBrO}_2]$, $x_2 = [\text{Br}^-]$, $x_3 = [\text{oxidized catalyst}]$, $x_4 = [\text{HOBr}]$, $x_5 = [\text{Br}_2]$, $x_6 = [\text{BrO}_2]$, and $x_7 = [\text{reduced catalyst}]$. Additionally $x_3 + x_7 = c_0$, where c_0 is the total concentration of the catalyst either in reduced or oxidized form, which remains constant over time. The catalyst, $\text{Ru}(\text{bpy})_3$, which has reduced $[\text{Ru}(\text{bpy})_3]^{2+}$ and oxidized $[\text{Ru}(\text{bpy})_3]^{3+}$ forms, is used in the photosensitive version of the BZ reaction. When there is no illumination, an idealized point BZ reactor, or alternatively the point FKN mechanism, behaves as a nonlinear oscillator. The photosensitive BZ reaction is inhibited partially or totally by electromagnetic radiation, which is accounted for by the presence of the function ϕ (defined in eq. (8)) in eqs. (2), (3) and (7) of the photosensitive FKN mechanism. Photoinhibition is mediated by bromide ion when the photosensitive catalyst $\text{Ru}(\text{bpy})_3$ is subjected to electromagnetic radiation ($\lambda = 450 \text{ nm}$) [16]. Here $b = [\text{BrCH}(\text{COOH})_2]$, $b_C = 0.05 \text{ M}$, and $k(I)$ is the reaction rate constant for light-mediated production of $[\text{Ru}(\text{bpy})_3]^{2+*}$ (photo-activated $[\text{Ru}(\text{bpy})_3]^{2+}$), which in turn promotes the production of bromide (see [19, 20] and [16] for details).

We perform numerical experiments to simulate the application of an inhibiting radiation beam of intensity I to the FKN oscillator in order to build a NFB signal. We assume that $k(I)$ is proportional to the inhibitory radiation intensity I according to eq. (9). Additionally, in eq. (10) we define I to be proportional to the concentration of oxidized catalyst ($x_3 = [\text{Ru}(\text{bpy})_3]^{3+}$) at $t - \tau$, where t is time and τ a time delay. q_1 and q_2 are appropriate constants for dimensional consistency. Thus, if x_3 (the oxidized catalyst concentration) increases, the inhibitory radiation illuminating the oscillator rises after a time delay τ , which in turn increases the concentration of bromide, thereby incrementing the inhibition on the reaction. The net result is that the radiation inhibition ϕ is dependent upon the time-delayed concentration of the species x_3 . We can tune the total and average radiation intensity by varying I .

We explore different scenarios as described below by applying feedback without time delay ($\tau = 0$) and with a time delay τ . When $\tau > 0$, we examine the delay effects and discover the preservation of key aspects of the FKN dynamics in the presence of feedback with constant (therefore deterministic) and with stochastic time delay. The constant time delay calculation is straightforward. We apply stochastic time delay as follows. At each solution

point while solving the system of differential equations (1–7), we control, through eq. (10), the time delay τ stochastically, choosing it from a given probability distribution. Hence τ is time-dependent. For stochastic time delay, we investigate two probability distributions, the normal distribution and the type I extreme value distribution (Gumbel distribution) of the minimum [57]. In the first case, τ is a random number taken from a normal distribution with known mean μ and standard deviation σ . In the second case τ is a random number taken from a Gumbel distribution with known location parameter α and scale parameter β according to the expression.

$$P(t - \tau) = \beta^{-1} \exp \left[\frac{t - \tau - \alpha}{\beta} - \exp \left(\frac{t - \tau - \alpha}{\beta} \right) \right]. \quad (11)$$

For each distribution we analyze six families, varying the width of the distribution by choosing six values of the standard deviation (σ) for the normal distribution and six values of the scale parameter (β) for the Gumbel distribution. For simplicity in exposition, we define the nominal time delay τ_N such that: *i*) $\tau = \tau_N$ when τ is constant, *ii*) $\mu = t - \tau_N$ when τ is stochastic and normally distributed, and *iii*) $\alpha = t - \tau_N$ when τ is stochastic and follows a Gumbel distribution. As a result, the distribution from which stochastic time delay, τ , is obtained, is constantly translated to the right at the same speed as t increases, *i.e.*, as each new solution point is calculated. The distribution is centered (μ for the normal and α for the Gumbel are located) behind t an amount τ_N . Feedback is applied only when $t \geq 397 + 2\tau_N$ s, and τ_N is at least five times larger than the width of the distribution ($\tau_N \geq 5\sigma, 5\beta$). As a consequence, only the tails of the distribution reach $\tau < 0$ and $\tau > t$ and the probability to obtain these values of τ is zero in our simulations.

The system of differential equations (1–7) is numerically integrated with MATLAB[®] variable order, multistep solver *ode15s*, which is based on the numerical differentiation formulas and optionally the backward differentiation formulas, methods particularly suitable to solve stiff problems [58–60].

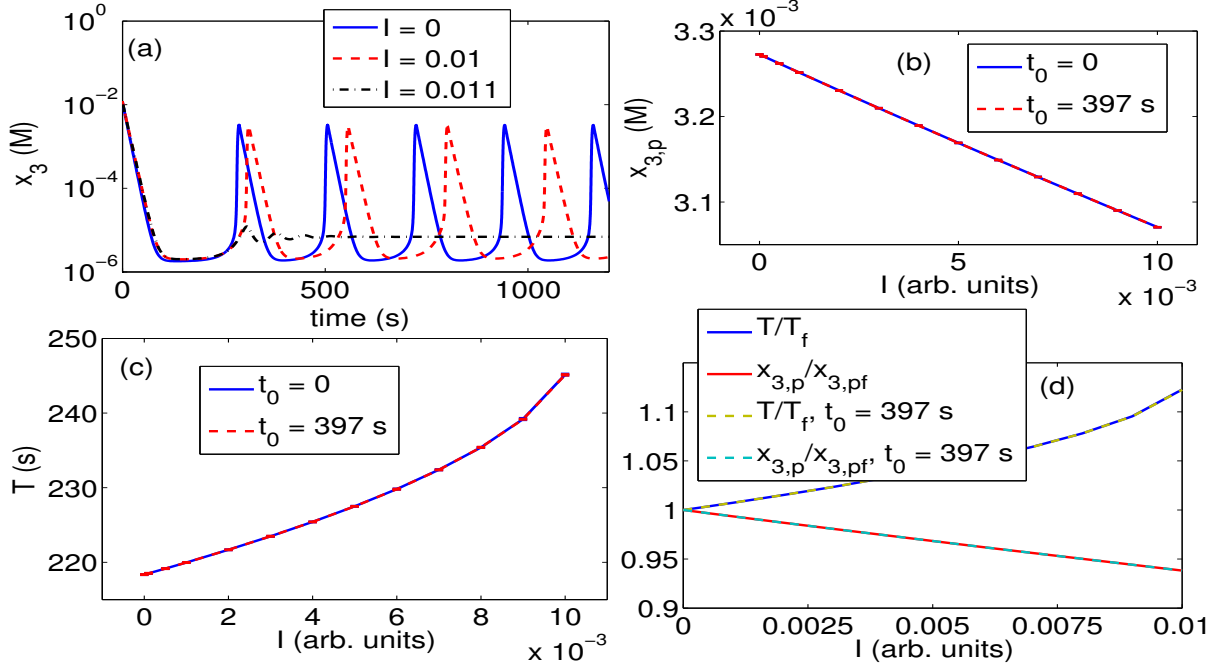


FIG. 1. Effects of radiation intensity on system dynamics. (a) Plot of x_3 time dependence for increased values of I . Critical radiation intensity $I_C = 0.011$ suppresses oscillatory dynamics. (b) Peak amplitude $x_{3,p}$ decreases linearly and (c) oscillation period T increases as inhibitory radiation increases. (d) T and $x_{3,p}$ time profiles normalized to free system (no-inhibition) values. Values of maximum amplitude en period are means averaged over several oscillatory cycles. Error bars (standard deviation) are barely noticeable in plots (b) and (c).

III. RESULTS AND DISCUSSION

First, we explore the role played by the average intensity level of the applied inhibiting radiation intensity, I . Due to the fundamental role played by the oxidized photosensitive catalyst x_3 , and since all seven FKN variables have the same oscillation frequency, we use x_3 to characterize the system dynamics. Figure 1a shows a comparison of the behavior of x_3 vs. time in the free system, *i.e.*, when there is no inhibitory radiation, and when inhibitory radiation is present. At $I = 0.01$, the oscillation period T is increased and the peak amplitude $x_{3,p}$ slightly decreased. Oscillations are suppressed at a critical average radiation intensity $I_C = 0.011$. Below this critical intensity, the main consequences of increasing inhibitory radiation intensity are the lengthening of the oscillation period and a slight decrease of the peak amplitude, with no significant effect on the shape of the curve. Figures 1b-d illustrate

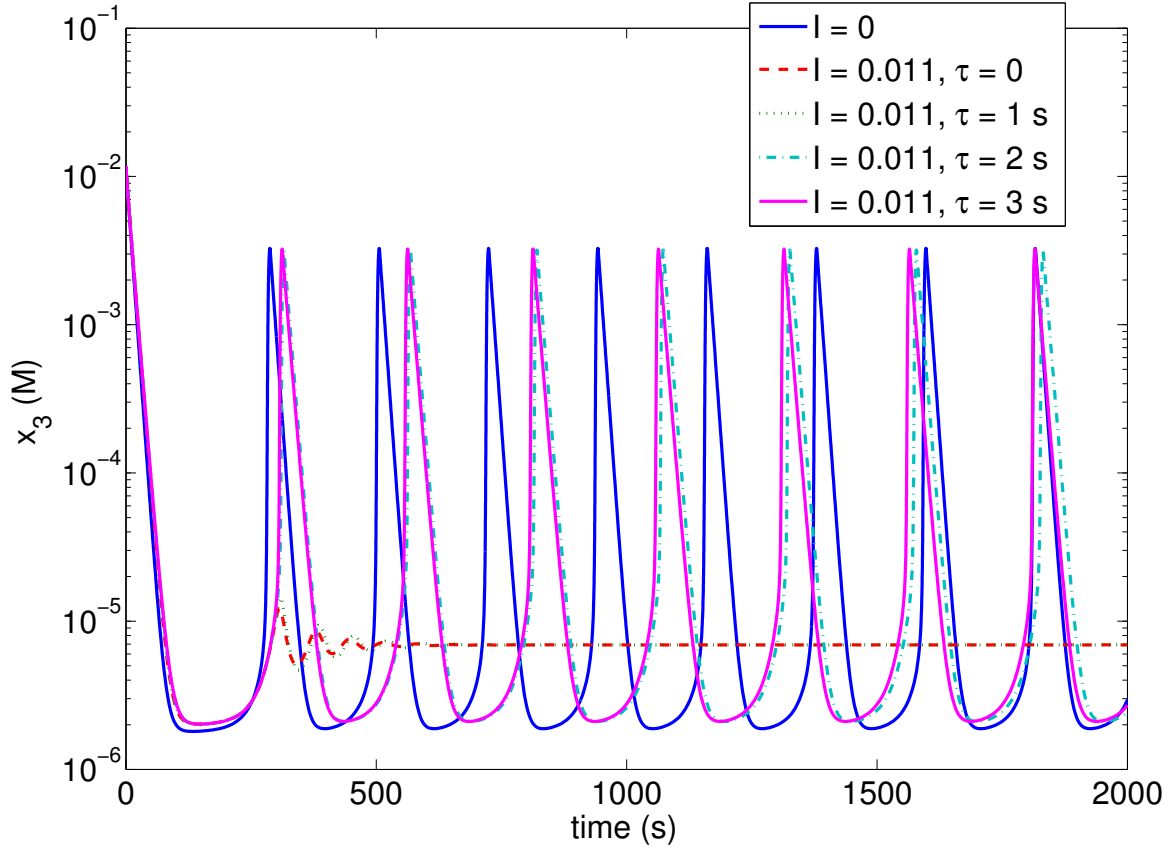


FIG. 2. Time dependence of x_3 at critical radiation intensity for increasing time-delayed feedback. The introduction of $\tau \geq 2$ s in feedback, results in system recovery of oscillatory dynamics at critical radiation intensity. The scale is the same for all plots.

these effects over a range of intensities. In Figure 1 b, c, and d, t_0 is the time at which the radiation feedback is turned on. The graphs show no difference when inhibitory radiation is turned on at time $t_0 = 0$, the time at which the simulation is initiated, or when the radiation is turned on at $t_0 = 397$ s. This result is unexpected, because transient behavior occurs during the first cycle of x_3 . We selected the time at the second minimum of x_3 ($t = 397$ s) because at this point regular periodic behavior is already established in the free system (Figure 1a, $I = 0$ curve). Even though there is no dependence on the time at which radiation inhibition is turned on, henceforth unless specified otherwise, we turn on inhibitory radiation at $t_0 = 397 + 2\tau$ s.

Next we introduce a time delay τ in the application of the feedback and examine its

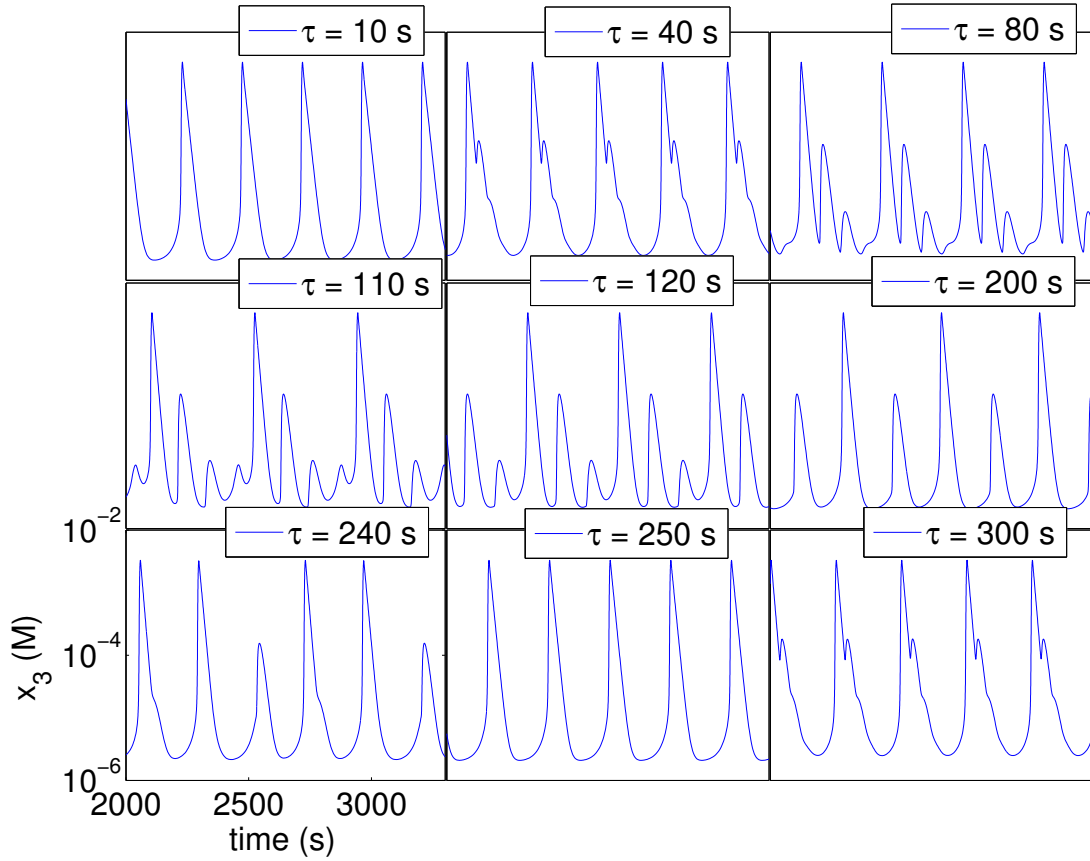


FIG. 3. Plot of x_3 vs. time as a function of increasing constant time delay (shown in the top right side in seconds). As time delay increases new peaks per cycle emerge, differentiate, and disappear. Note that free system dynamics appears to be recovered at $\tau = 250$ s, compare with $\tau = 10$ s and with Figure 1a curve $I = 0$. Also note that system behaves similarly at $\tau = 40$ s and $\tau = 300$ s.

effects. First we consider constant, *i.e.*, deterministic time delay. Figure 2 shows x_3 vs. time at the critical inhibiting radiation for different values of τ . As previously noted, oscillations are suppressed at the critical radiation intensity in the absence of time delay. Interestingly, the system recovers its oscillatory dynamics if the inhibiting critical radiation is applied with a time delay. For $\tau \geq 2$ s, system oscillations are recovered with no significant change in the x_3 peak amplitude and time profile.

We now consider how the system dynamics is modified when inhibitory feedback is applied at a subcritical radiation intensity with constant time delay. Figure 3 shows nine plots of x_3 vs. time at $I = 0.01$ for increasing values of τ . These plots correspond to the different

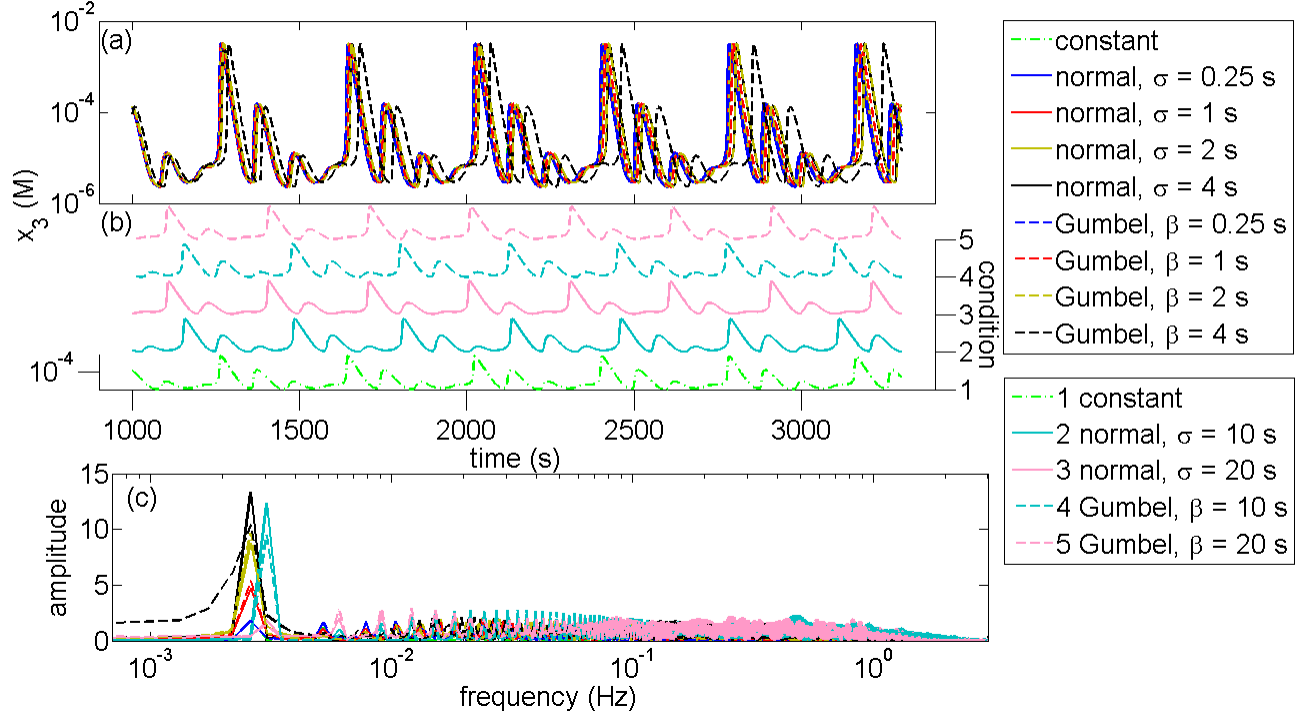


FIG. 4. Real, (a) and (b), and Fourier (c) space plots of x_3 for all time delay conditions investigated at $\tau_N = 100$ s. Real space profiles exhibit closely similar dynamic behavior for all time delay conditions. Fourier analysis shows the concordance of the main and some secondary frequency components roughly divided into small and large dispersions. Plots of x_3 at small (a) and large (b) dispersion exhibit essentially equal amplitude.

characteristic time profiles exhibited by x_3 as a function of time-delayed feedback. The time window for each plot was selected after the transients died out and the system exhibited regular periodic behavior.

The figure shows significant changes in the x_3 time profile as τ increases. At $\tau = 40, 80, 110, 120, 200$, and 240 s, we observe more complex time profiles, which contain 2, 3, 4, 3, 2, and 3 peaks per cycle, respectively. Interestingly, at $\tau = 250$ s, the waveform of the system at $\tau \leq 10$ s is recovered (which essentially is the same of the free system), with one peak per cycle. The oscillation period of 245 s, is the same as that at $\tau = 10$ s (Figure 9). The last plot at $\tau = 300$ s resembles that at $\tau = 40$ s with a similar period. This could suggest that system behavior is periodic in τ with a period of about 250 s. See discussion of figure 9 on this issue.

Finally, we investigated the role of negative feedback with stochastic time delay at a subcritical radiation intensity ($I = 0.01$). Stochastic time delays with normal and Gumbel probability distributions were used. In choosing the normal and Gumbel distributions, one of our purposes was to compare the effects of stochastic time delay from a symmetric and a nonsymmetric distribution. The dispersions applied were $\sigma = 0.25, 1, 2, 4, 10$, and 20 s for the normal distribution and $\beta = 0.25, 1, 2, 4, 10$, and 20 s for Gumbel distribution. Figure 4 shows plots of x_3 in the real, (a) and (b), and Fourier (c) spaces at $\tau_N = 100$ s for the 13 conditions of time-delayed feedback investigated: one constant and the 12 stochastic just described. Again, the frame has been chosen after transients, once periodic behavior is established. In real space, all plots exhibit outstanding similar dynamics. We observe good matching between plots for dispersions of 4 s and below for both distributions. At large dispersion, 10 and 20 s (b), the only important difference between plots is in frequency and/or phase. The first peaks, which occur at the same location in Fourier space in most of the plots, correspond to the major frequency component. The slight frequency difference at low dispersion (≤ 4 s), noticeable in real space, is not evidenced in the peak's location in Fourier space, due to the large scale of the plot. However, at large dispersion (≥ 10 s) the frequency is significantly larger, as evidenced by the shift of the main peaks in the Fourier transform. Additionally, a large set of lower amplitude frequency components is apparent in the Fourier domain. Figure 5 shows an analogous plot at $\tau_N = 200$ s. Again, there is a remarkable match of dynamic behavior in real space, (a) and (b) parts of the figure, for all the conditions investigated. The most significant differences occur in phase for large dispersions (b). Primary and several secondary frequency components exhibit impressive agreement as shown in plots of the Fourier domain (c), for all conditions.

The same trend of closely matching dynamics for the entire set of time-delayed feedback conditions investigated is observed for the complete interval of nominal time delay explored ($10 \text{ s} \leq \tau_N \leq 300 \text{ s}$). Time profile, frequency and mainly phase exhibit growing differences as the dispersion in time delay increases. The similarity is particularly noticeable at low time delay dispersion (≤ 4 s) with the striking exceptions of $\tau_N = 110$ and 240 s. Figure 6 shows the case of $\tau_N = 110$ s. In real space (a), only plots 1, 2, 3, and 8 (constant, $\sigma = 0.25$ s, $\sigma = 1$ s, and $\beta = 0.25$ s) exhibit near-perfect agreement in every aspect of their dynamics.

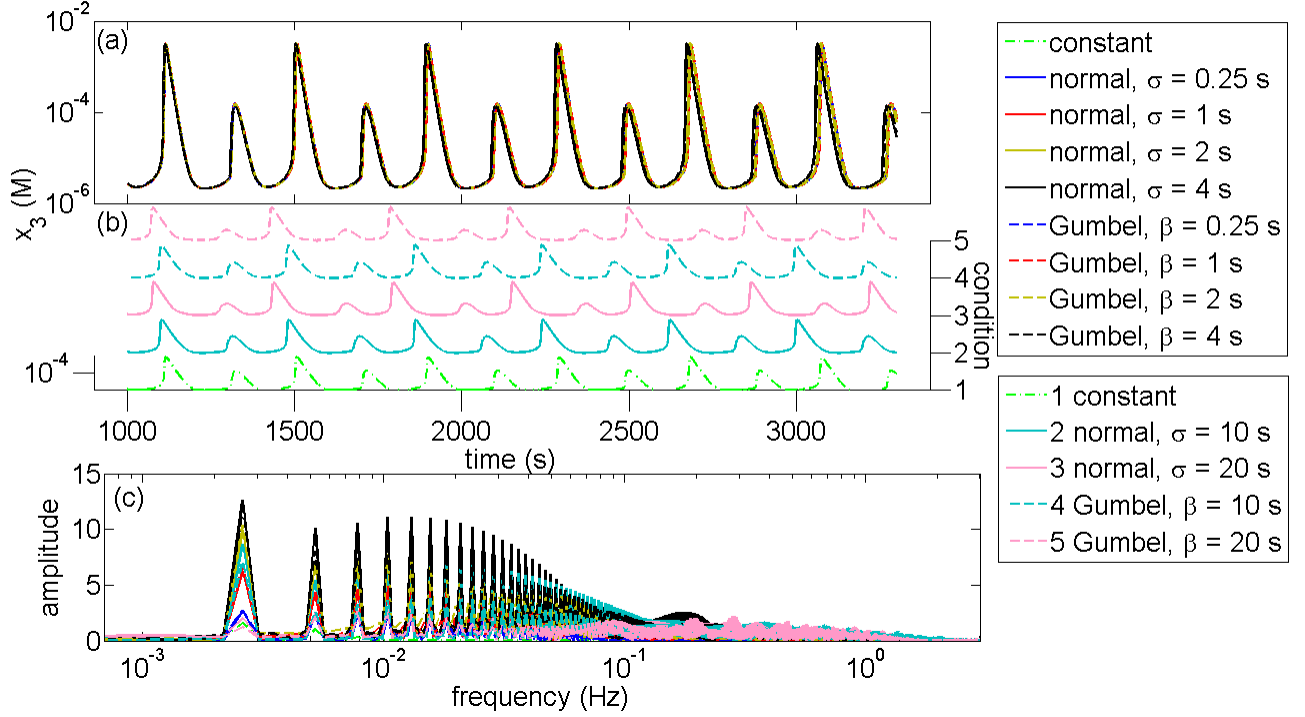


FIG. 5. Real, (a) and (b), and Fourier (c) domains of x_3 state at $\tau_N = 200$ s for all time delay conditions explored. As in the previous Figure, the agreement between all plots is remarkable. Plots of x_3 at small (a) and large (b) dispersion exhibit essentially equal amplitude.

These plots present four maxima (one global and three local) per oscillation cycle in contrast with three or two for the remaining conditions with periodic behavior. The transition from four to three maxima per oscillation occurs at $\sigma = 2$ s in the normal distribution (plot 4). This plot appears to be aperiodic with an apparently random peak sequence 4-3-3-4-3. An analogous transition in the number of peaks per oscillation with aperiodic behavior is observed in plot 9, (Gumbel distribution $\beta = 1$ s) which has the peak sequence 3-4-4-4-3. In both cases (normal and Gumbel distributions) two different runs with identical simulation conditions but different random sequences of time delays, generated different peak sequences. One outcome of the increase in time delay dispersion is the suppression of secondary peaks in the real space dynamics and a decrease in oscillation period. This is revealed in Fourier space (b), where plots for $\sigma \geq 4$ s and $\beta \geq 2$ s show the main frequency component peaks shifted to the right.

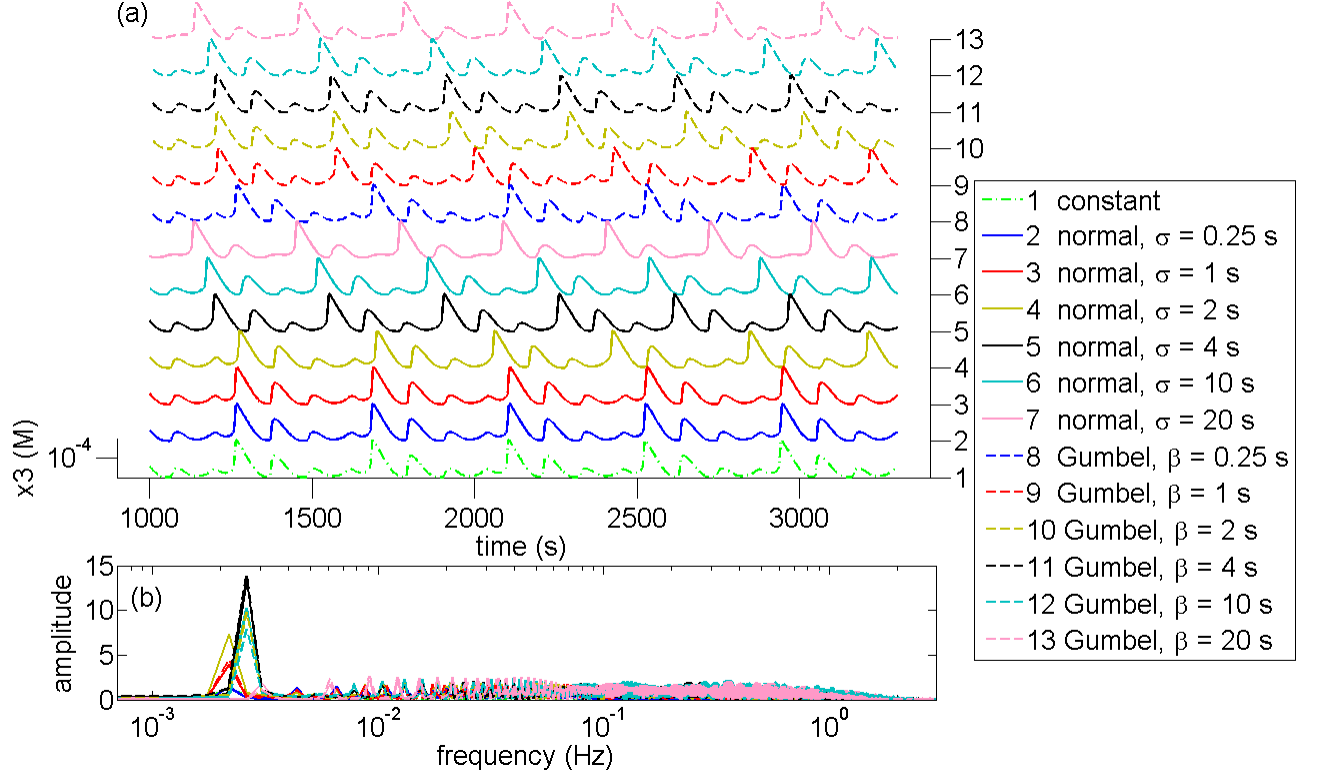


FIG. 6. Plots of x_3 in real (a), and Fourier (b) spaces for all conditions of time delay investigated at $\tau_N = 110$ s. Periodicity is preserved in curves 1, 2, 3, 5, and 7. Plots 1, 2, 3, and 5 still exhibit a close match while plot 7 shows a larger frequency, evidenced in the Fourier domain, where the frequency component peaks are shifted to the right. Plots 4 and 6 appears to be aperiodic functions, though they still exhibit main frequency components very similar to those of the periodic plots.

In order to have a quantitative measure of the match between x_3 waveforms subjected to feedback with stochastic and constant time delays independent of frequency and phase, we define the quantity q_i as

$$q_i = \frac{\int_0^1 |v_i - u| dt}{\int_0^1 u dt}, \quad i = 1, 2, \dots, 12. \quad (12)$$

where $u(t) = x_3(Tt + t_M)$ under constant time delay and $v_i(t) = x_{3i}(T_i t + t_{Mi})$ under stochastic time delay (the index i specifies which form of stochastic time delay is used, see Figure 7); $T(T_i)$ is the oscillation period at constant(stochastic) time delay and $t_M(t_{Mi})$ is the time of the penultimate peak when time delay is constant(stochastic). Equation (12) integrates the absolute difference between frequency-normalized states x_3 under stochastic

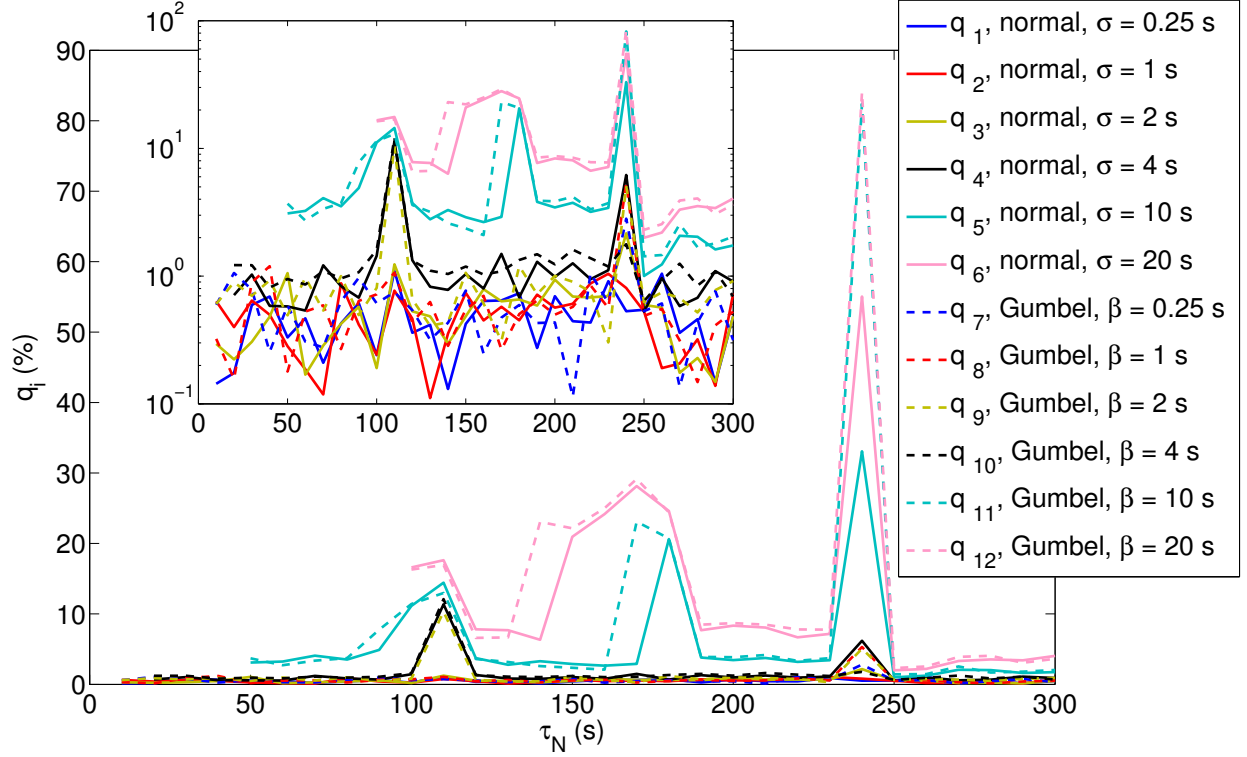


FIG. 7. Plot of q_i vs. τ_N shows that for all conditions of time delay studied q_i remains below 30% for nearly all τ_N , except near $\tau_N = 240$ s. The inset shows a logarithmic plot of the same data.

and constant time delay, over one oscillation cycle (the last simulated), with their phases matched, and normalizes this integrated difference to the one-cycle integral of u .

Figure 7 shows q_i as a function of nominal time delay for all conditions of stochastic time-delayed feedback investigated. Remarkably, there is only one condition of nominal time delay, $\tau_N = 240$ s, at which q_i is larger than 30%. This occurs solely for the largest dispersions in time delay explored (≥ 10 s). For discussion purposes and based on the figure, we define low (≤ 4 s) and high (≥ 10 s) time delay dispersions for the behavior of q_i . At low dispersion q_i is always less than 2% over the entire range of nominal time delay, with two exceptions $\tau_N = 110$ and 240 s. The case of $\tau_N = 110$ s has been discussed in Figure 6. A similar situation occurs at $\tau_N = 240$ s. Even in these cases, q_i is close to 10%. At large dispersion, q_i increases moderately, remaining below 30% with the exception mentioned above. The largest q_i values occur at the largest dispersion explored, 20 s, and the Gumbel distribution generally exhibits larger q_i than the normal distribution. There are three intervals that contain large

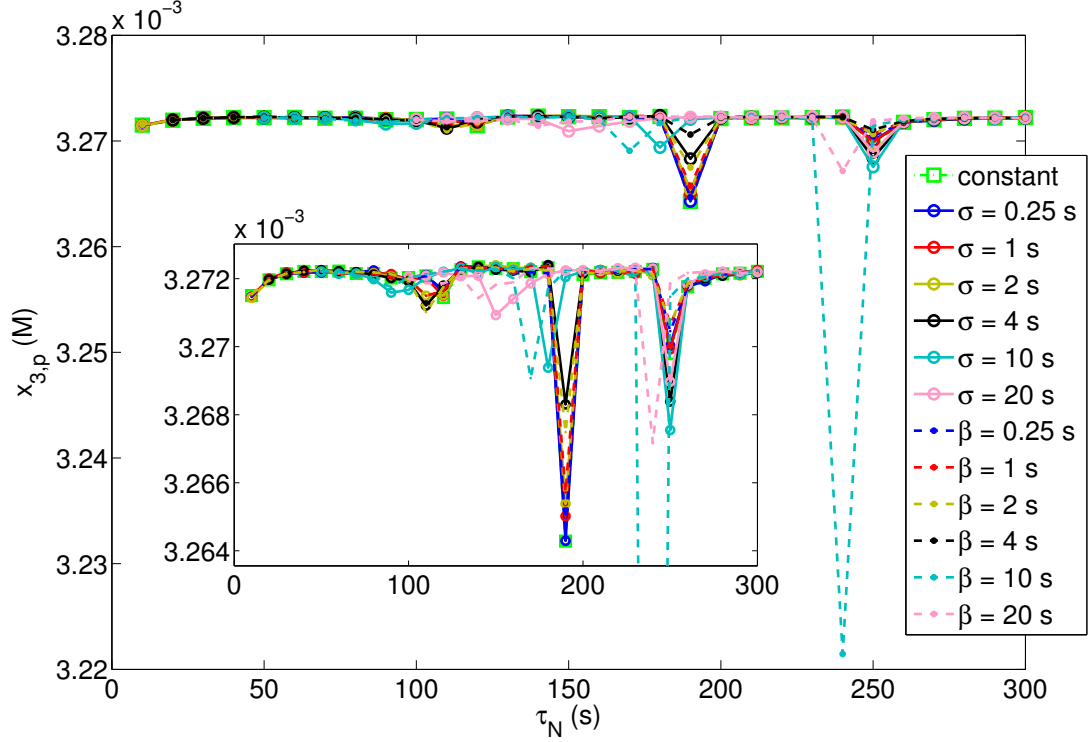


FIG. 8. Plot of x_3 peak amplitude, $x_{3,p}$ as a function of τ_N . The plot shows a remarkable agreement between all time-delayed feedback conditions. A logarithmic plot of these data is shown in the inset.

values of q_i : $\tau_N = 100 - 110$ s, $\tau_N = 130 - 180$ s and $\tau_N = 240$ s.

Finally, we present results for the signal x_3 amplitude (maxima) and period (frequency). Figure 8 shows a plot of signal amplitude, $x_{3,p}$, *vs.* nominal time delay. The plot compares constant and all stochastic time-delayed feedback conditions. Besides small local differences, there is a surprising match for the whole set of curves. The largest mismatch, which occurs at $\tau_N = 240$ s for $\beta = 10$ s, is less than 1.6% relative to constant time delay. There are three intervals where noticeable decrements in peak amplitude occur (including conditions at constant and small dispersion stochastic time delay), at or around $\tau_N = 110$ s, $\tau_N = 140 - 190$ s, and $\tau_N = 240 - 250$ s. In all three cases there is a decrease in the number of maxima per oscillation cycle of the state x_3 (see Figure 3). The number of peaks per cycle decreases from four to three peaks at $\tau_N \simeq 110$ s, from three to two at $\tau_N = 190$ s, and from three to one $\tau_N = 250$ s (in this case the number of peaks increases from two to three at $\tau_N = 240$ s). Notice that secondary (local) maxima fade or disappear as the dispersion increases, as seen

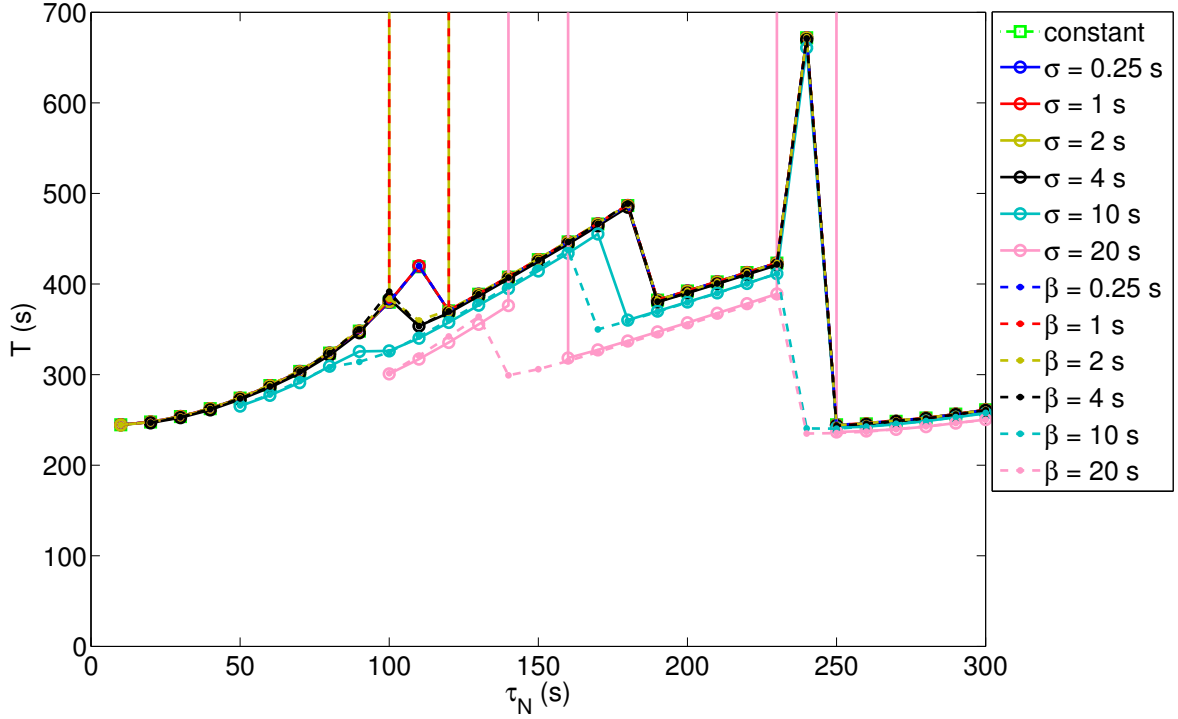


FIG. 9. Oscillation period T as a function of τ_N . As in Figure 8, the curves exhibit a remarkable match for all conditions of time-delayed feedback applied.

in Figures 4 and 6. We emphasize that the intervals mentioned roughly correspond to the peaks in Figure 7.

Figure 9 shows the oscillation period as a function of the nominal time delay. The signal exhibits four continuous regions of increasing period as τ_N increases. In the boundary between these regions there are intervals (three) which suggest the existence of a discontinuity. These intervals loosely coincide with a) the regions where the x_3 amplitude and number of peaks per cycle decrease and with b) the peaks of Figure 7, *i.e.*, at $\tau_N \simeq 140 - 190$, and 240 s. Two regions of period increase exhibit non-linear behavior (first and fourth regions from left to right) and two exhibit linear behavior (regions two and three). We find four cases at which state x_3 does not exhibit periodic behavior, marked with infinite period in the Figure (vertical lines). The cases are: 1) $\sigma = 2$ s, $\tau_N = 110$ s; 2) $\beta = 1$ s, $\tau_N = 110$ s; 3) $\sigma = 20$ s, $\tau_N = 150$ s; and 4) $\sigma = 20$ s, $\tau_N = 240$ s. These cases lie within the intervals described. As discussed in figure 3, the recovering of the oscillation period and waveform at $\tau_N = 250$ s

suggests that system behavior is periodic in time delay τ . However, we note in figure 9 that the first region of the plots ($10 \text{ s} \leq \tau_N \leq 60 \text{ s}$) grows faster and have a larger first derivative than the last region ($250 \text{ s} \leq \tau_N \leq 300 \text{ s}$).

IV. CONCLUSION

We have investigated the effect of time-delayed negative feedback on a point photosensitive FKN oscillator by means of simulated inhibitory radiation. We find that increasing the radiation intensity with no time delay lengthens the oscillatory period and lowers the peak amplitude of the oxidized photosensitive catalyst concentration profile. At a critical intensity of illumination, oscillatory dynamics is suppressed. These observations can be attributed to the production of bromide, which in turn inhibits the oxidation of $[\text{Ru}(\text{bpy})_3]^{2+}$. If the concentration of the inhibitor increases, the time needed for its concentration to decrease to values compatible with oxidation transitions will also increase; thus, the refractory time and therefore the oscillation period should also increase. Similarly, at increased inhibitor concentrations, the maximum concentration of oxidized catalyst should decrease, as the available activator is partially depleted relative to the inhibition-free case. We also observe that the response of the system is the same whether non-delayed feedback is initiated during transient behavior or once periodic behavior is established, and that introduction of delayed feedback allows recovery of oscillatory behavior in the presence of a radiation level that suppresses oscillation in the absence of delay.

Our main objective is to investigate the effects of incorporating a stochastic time delay in the feedback. We compare the response of the FKN oscillator under constant *versus* stochastic time-delayed feedback. Investigation with stochastic time delay included two probability distributions, a symmetric normal and a non-symmetric Gumbel, with six values of parameter dispersion for each. The FKN model exhibits a surprising amplitude and frequency match for low dispersion ($\leq 4 \text{ s}$) in the probability distribution of the time-delayed feedback over a wide interval of time delay values, which spanned more than 1.3 times the natural oscillation period of the free system ($10 \text{ s} \leq \tau_N \leq 300 \text{ s}$). Additionally, there is a striking agreement in the time profiles for the situations described. The amplitude

and period of x_3 decrease or show a significant curvature change in three intervals of the nominal time delay: 1) $\tau_N = 90 - 120$ s, 2) $\tau_N = 140 - 190$ s, and 3) $\tau_N = 240 - 250$ s. The time delay (nominal) at which the transition occurs shifts towards lower values as the dispersion in the probability distribution of stochastic time delay increases. These regions closely coincide with those at which q_i exhibits bumps or peaks, *i.e.*, when the waveform of x_3 under stochastic time delay feedback diverges most from that under constant delay. In these parameter regions, one secondary peak in the oscillation cycle of x_3 fades and disappears, and the signal exhibits aperiodic behavior in some cases when time delay is stochastic.

Experimental implementation of this investigation will be carried out in future work. This can be accomplished with droplets of the BZ reaction prepared in the oscillatory regime and subjected to an inhibitory light beam [11, 61]. A PC connected to a CCD video camera can evaluate, from droplet image brightness, the concentration of oxidized catalyst in the drops and tune accordingly the beam intensity with an appropriate constant or stochastic time delay.

V. ACKNOWLEDGMENTS

I.R.E. acknowledges support from the U.S. National Science Foundation through Grant No. CHE-1362477.

-
- [1] B. P. Belousov, in *Collection of Short Papers on Radiation Medicine* (Medgiz: Moscow, 1959).
 - [2] A. M. Zhabotinsky, Proc. Acad. Sci. USSR **157**, 392 (1964).
 - [3] A. N. Zaikin and A. M. Zhabotinsky, Nature **225**, 535 (1970).
 - [4] A. T. Winfree, Science **175**, 634 (1972).
 - [5] R. Kapral and K. Showalter, eds., *Chemical Waves and Patterns* (Dordrecht: Kluwer, 1995).
 - [6] I. Prigogine, *From Being to Becoming: Time and Complexity in the Physical Sciences* (W. H. Freeman and Company, 1980).
 - [7] J. Lechleiter, S. Girard, E. Peralta, and D. Clapham, Science **252**, 123 (1991).

- [8] S. Girard, A. Lückhoff, J. Lechleiter, J. Sneyd, and D. Clapham, *Biophys. J.* **61**, 509 (1992).
- [9] A. M. Turing, *Philos. T. Roy. Soc.* **237**, 37 (1952).
- [10] V. Castets, E. Dulos, J. Boissonade, and P. De Kepper, *Phys. Rev. Lett.* **64**, 2953 (1990).
- [11] N. Tompkins, N. Li, C. Girabawe, M. Heymann, G. B. Ermentrout, I. R. Epstein, and S. Fraden, *P. Natl. Acad. Sci. U.S.A.* **111**, 4397 (2014).
- [12] A. F. Taylor, M. R. Tinsley, F. Wang, Z. Huang, and K. Showalter, *Science* **323**, 614 (2009).
- [13] H. Fukuda, N. Tamari, H. Morimura, and S. Kai, *J. Phys. Chem. A* **109**, 11250 (2005).
- [14] B. T. Ginn, B. Steinbock, M. Kahveci, and O. Steinbock, *J. Phys. Chem. A* **108**, 1325 (2004).
- [15] L. Kuhnert, K. I. Agladze, and V. I. Krinsky, *Nature* **337**, 244 (1989).
- [16] S. Kádár, T. Amemiya, and K. Showalter, *J. Phys. Chem. A* **101**, 8200 (1997).
- [17] R. J. Field, E. Körös, and R. M. Noyes, *J. Am. Chem. Soc.* **94**, 8649 (1972).
- [18] P. Ruoff, *J. Phys. Chem.* **88**, 2851 (1984).
- [19] V. K. Vanag, A. M. Zhabotinsky, and I. R. Epstein, *J. Phys. Chem. A* **104**, 8207 (2000).
- [20] V. K. Vanag and I. R. Epstein, *J. Chem. Phys.* **131**, 104512 (2009).
- [21] K. Pyragas and A. Tamaševičius, *Phys. Lett. A* **180**, 99 (1993).
- [22] K. Pyragas, *Phil. Trans. R. Soc. A* **364**, 2309 (2006).
- [23] E. Ott, C. Grebogi, and J. A. Yorke, *Phys. Rev. Lett.* **64**, 1196 (1990).
- [24] K. Pyragas, *Phys. Lett. A* **170**, 421 (1992).
- [25] V. Flunkert and E. Schöll, *Phys. Rev. E* **76**, 066202 (2007).
- [26] M. G. Rosenblum and A. S. Pikovsky, *Phys. Rev. Lett.* **92**, 114102 (2004).
- [27] S. A. Campbell, J. Blair, T. Ohira, and J. Milton, *Chaos* **5**, 640 (1995).
- [28] F. Lin and J. Liu, *IEEE J. Quantum Electron.* **39**, 562 (2003).
- [29] F. W. Schneider, R. Blittersdorf, A. Förster, T. Hauck, D. Lebender, and J. Müller, *J. Phys. Chem.* **97**, 12244 (1993).
- [30] M. Bestehorn, E. V. Grigorieva, and S. A. Kaschenko, *Phys. Rev. E* **70**, 026202 (2004).
- [31] Y. N. Kyrychko, K. Blyuss, S. Hogan, and E. Schöll, *Chaos* **19**, 043126 (2009).
- [32] Q. Li and H. Hu, *J. Chem. Phys.* **127**, 154510 (2007).
- [33] H. Hu, X. Li, Z. Fang, X. Fu, L. Ji, and Q. Li, *Chem. Phys.* **371**, 60 (2010).
- [34] S. V. Gurevich, *Phys. Rev. E* **87**, 052922 (2013).

- [35] R. Iri, Y. Tonosaki, K. Shitara, and T. Ohta, J. Phys. Soc. Jpn. **83**, 024001 (2014).
- [36] C. Tian and L. Zhang, Phys. Rev. E **88**, 012713 (2013).
- [37] D. Goldobin, M. G. Rosenblum, and A. Pikovsky, Phys. Rev. E **67**, 06119 (2003).
- [38] D. Arsenijević, M. Kleinert, and D. Bimberg, Appl. Phys. Lett. **103**, 231101 (2013).
- [39] M. C. Soriano, J. Garca-Ojalvo, C. R. Mirasso, and I. Fischer, Rev. Mod. Phys. **85**, 421 (2013).
- [40] R. Vicente, L. L. Gollo, C. R. Mirasso, I. Fischer, and P. Gordon, P. Natl. Acad. Sci. U.S.A. **105**, 17157 (2008).
- [41] C. Masoller, Phys. Rev. Lett. **88**, 034102 (2002).
- [42] N. B. Janson, A. G. Balanov, and E. Schöll, Phys. Rev. Lett. **93**, 010601 (2004).
- [43] L. Jaurigue, E. Schöll, and K. Lüdge, Phys. Rev. Lett. **117**, 154101 (2016).
- [44] Y. Kanevsky and A. A. Nepomnyashchy, Phys. Rev. E **76**, 066305 (2007).
- [45] B. Lindner, B. Doiron, and A. Longtin, Phys. Rev. E **72**, 061919 (2005).
- [46] S. Gil and A. S. Mikhailov, Phys. Rev. E **79**, 026219 (2009).
- [47] V. K. Vanag, A. M. Zhabotinsky, and I. R. Epstein, J. Phys. Chem. A **104**, 11566 (2000).
- [48] V. K. Vanag, L. Yang, M. Dolnik, A. M. Zhabotinsky, and I. R. Epstein, Nature **389**, 406 (2000).
- [49] A. S. Mikhailov and K. Showalter, Phys. Rep. **425**, 79 (2006).
- [50] W. Wang, I. Z. Kiss, and J. Hudson, Ind. Eng. Chem. Res. **41**, 330 (2002).
- [51] S. Yanchuk and G. Giacomelli, Phys. Rev. Lett. **112**, 174103 (2014).
- [52] J. A. Kromer, B. Lindner, and L. Schimansky-Geier, Phys. Rev. E **89**, 032138 (2014).
- [53] A. Gjurchinovski and V. Urumov, Phys. Rev. E **81**, 016209 (2010).
- [54] M. Toiya, V. K. Vanag, and I. R. Epstein, Angew. Chem. Int. Ed. **47**, 7753 (2008).
- [55] M. Toiya, H. O. González-Ochoa, V. K. Vanag, S. Fraden, and I. R. Epstein, J. Phys. Chem. Lett. **1**, 1241 (2010).
- [56] A. N. Zaikin and A. M. Zhabotinsky, in *Biological and Biochemical Oscillators*, edited by B. Chance, E. K. Pye, A. K. Ghosh, and B. Hess (Academic Press: New York, 1973).
- [57] R. D. Reiss and M. Thomas, *Statistical Analysis of Extreme Values*, Handbook on Statistical Distributions for Experimentalists (Birkhäuser Verlag, University of Stockholm, 2007).

- [58] L. F. Shampine and M. W. Reichelt, SIAM J. Sci. Comput. **18**, 1 (1997).
- [59] L. F. Shampine, M. W. Reichelt, and J. A. Kierzenka, SIAM Rev. **41**, 538 (1999).
- [60] R. W. Klopfenstein, RCA Rev. **32**, 447 (1971).
- [61] J. Delgado, N. Li, M. Leda, H. O. González-Ochoa, S. Fraden, and I. R. Epstein, Soft Matter **7**, 3155 (2011).